Available online at www.sciencedirect.com
ScienceDirect
Geochimica et Cosmochimica Acta 73 (2009) 1696–1710
Geochimica et Cosmochimica Acta
www.elsevier.com/locate/gca

Solution behavior of reduced C—O—H volatiles in silicate melts at high pressure and temperature

Bjorn O. Mysen [a,*], Marilyn L. Fogel [a], Penny L. Morrill [b], George D. Cody [a]

[a] Geophysical Laboratory, Carnegie Institution of Washington, 5251 Broad Branch Road, NW, Washington, DC 20015-1305, USA
[b] Dept. Earth Sci., Memorial University of Newfoundland, Canada

Received 18 February 2008; accepted in revised form 19 December 2008; available online 30 December 2008

Abstract

The solubility and solution mechanisms of reduced C—O—H volatiles in Na_2O—SiO_2 melts in equilibrium with a ($H_2 + CH_4$) fluid at the hydrogen fugacity defined by the iron-wüstite + H_2O buffer [f_{H2}(IW)] have been determined as a function of pressure (1–2.5 GPa) and silicate melt polymerization (NBO/Si: nonbridging oxygen per silicon) at 1400 °C. The solubility, calculated as CH_4, increases from ~0.2 wt% to ~0.5 wt% in the melt NBO/Si-range ~0.4 to ~1.0. The solubility is not significantly pressure-dependent, probably because f_{H2}(IW) in the 1–2.5 GPa range does not vary greatly with pressure. Carbon isotope fractionation between methane-saturated melts and ($H_2 + CH_4$) fluid varied by ~14‰ in the NBO/Si-range of these melts.

The (C..H) and (O..H) speciation in the quenched melts was determined with Raman and ^{1}H MAS NMR spectroscopy. The dominant (C..H)-bearing complexes are molecular methane, CH_4, and a complex or functional group that includes entities with C≡C—H bonding. Minor abundance of complexes that include Si—O—CH_3 bonding is tentatively identified in some melts. There is no spectroscopic evidence for Si—C or Si—CH_3. Raman spectra indicate silicate melt depolymerization (increasing NBO/Si). The $[CH_4/C{\equiv}C{-}H]^{melt}$ abundance ratio is positively correlated with NBO/Si, which is interpreted to suggest that the (C≡C—H)-containing structural entity is bonded to the silicate melt network structure via its nonbridging oxygen. The ~14‰ carbon isotope fractionation change between fluid and melt is because of the speciation changes of carbon in the melt.

1. INTRODUCTION

The formation and evolution of the geo-, hydro-, and atmosphere are closely linked to the behavior of volatiles in the Earth's interior (e.g., Kasting et al., 1993; Jambon, 1994; Holloway, 1998; Tolstikhin and Marty, 1998; Deines, 2002; Cartigny and Ader, 2003). Volatiles in the C—O—H system (H_2O, H_2, CO_2, CO, CH_4) dominate in the silicate Earth (e.g., Jambon, 1994). Characterization of the solubility and solution mechanisms of C—O—H volatile components in silicate melts is, therefore, a necessary part of the information needed to describe formation and evolution of solid Earth.

The solubility and solution mechanisms of C—O—H volatiles in silicate melts depend on pressure, temperature, redox conditions, and silicate melt and C—O—H fluid composition (see, for example, Holloway and Blank, 1994; Mysen and Richet, 2005; for reviews of relevant information). Redox conditions are important because C—O—H speciation and abundance vary in the oxygen fugacity (f_{O2}) range within the Earth (e.g., Eggler and Baker, 1982; Kasting et al., 1993; Holloway and Blank, 1994; Kadik et al., 2004; McCammon, 2005). Moreover, the redox conditions have changed during the Earth's history from perhaps as much as 2–3 orders of magnitude below that of the iron-wüstite (IW) equilibrium during the core-forming stage (e.g., O'Neill, 1991; Righter et al., 1997; O'Neill et al.,

* Corresponding author.
E-mail address: bmysen@ciw.edu (B.O. Mysen).

0016-7037/$ - see front matter © 2008 Elsevier Ltd. All rights reserved.
doi:10.1016/j.gca.2008.12.016

1998; Righter and Drake, 1999; Gessmann and Rubie, 2000; Chabot and Agee, 2003) to typically within 1–2 orders of magnitude of the quartz-fayalite-magnetite (QFM) buffer in current upper mantle (e.g., Mattioli and Wood, 1986; O'Neill, 1991; Canil, 2002; McCammon, 2005). Such an f_{O2}-evolution will result in C—O—H volatile species changes from dominantly H_2, H_2O, and CH_4 to dominantly H_2O and CO_2. Of course, redox conditions of the silicate Earth even today vary significantly.

In the C—O—H system of volatiles, the solubility and solution behavior of H_2O in silicate melts is reasonably well known, at least under upper mantle pressure and temperature conditions. The solubility and solution behavior of H_2 and CH_4 under similar conditions are, however, are less well established (Eggler and Baker, 1982; Holloway and Jakobsson, 1986; Luth and Boettcher, 1986; Luth et al., 1987; Taylor and Green, 1987; Kadik et al., 2004). Methane solubility and solution mechanisms at high pressure and temperature is fundamental to describe *how* reduced C may be sequestered in melts in the Earth's mantle particularly during its earliest periods of core formation and large-scale magma oceans, *how* carbon isotope fractionation between fluid and melt phases may vary with carbon speciation in thee phases, and *how* the physicochemical properties of silicate melts at high pressure are affected by CH_4 in solution. Here, we will focus on methane solubility in melts, carbon isotope fractionation between melt and fluid, and solution mechanisms of C—O—H fluids in silicate melts.

2. EXPERIMENTAL METHODS

Silicate starting compositions were in the Na_2O—SiO_2 system with nominal Na/Si = 0.4–1.0. The compositions are denoted NS5 (nominal Na/Si = 0.4), NS4 (nominal Na/Si = 0.5), N3S8 (nominal Na/Si = 0.75), and NS2 (nominal Na/Si = 1). For volatile-free melts, the Na/Si ratio equals NBO/Si (nonbridging oxygen/silicon) provided that Si^{4+} is in 4-fold coordination. In the 1–2.5 GPa pressure range of the present study, the NBO/Si was considered equal to Na/Si although 1–2% 5- or 6-fold coordinated Si has been suggested at pressures as low as 1.9 GPa (Xue et al., 1991). Major fractions of high-coordinated Si are unlikely at pressures less than about 10 GPa (Lee et al., 2003). Even for the most depolymerized melt studied here, NS2, 2% of the Si in 5- or 6-fold coordination translates to a relative uncertainty of NBO/Si of about 2.5%.

Starting materials were prepared in two stages. First, volatile-free Na-silicate glass starting materials were made by grinding and mixing ~1 g of SiO_2 and Na_2CO_3 under alcohol for 1 h. Glasses were formed from these mixtures by heating the oxide + carbonate mixture at 1 °C/min to above the Na_2CO_3 decarbonation temperature, and then brought to about 100 °C above their liquidus temperatures where the melt was kept for 1 h. This melt was transformed to glass by quenching in liquid water. The cooling rate during quenching to glass is on the order of 100–200 °C/s. Second, melts at high pressure (1–2.5 GPa) and temperature (1400 °C) were synthesized from mixtures of these volatile-free glasses together with $Si_5C_{12}H_{36}$ (tetrakis-silane) and H_2O. Tetrakis-silane reacts with H_2O to form SiO_2, CH_4 and H_2 at the experimental conditions:

$$Si_5C_{12}H_{36} + 10\ H_2O = 5\ SiO_2 + 12\ CH_4 + 4\ H_2 \quad (1)$$

The silicate/tetrakis-silane/H_2O proportions of the starting mixtures were such that at high temperature and pressure, the silicate had the desired Na/Si. Under the high-temperature/-pressure conditions, there was approximately 5 wt% fluid and 95 wt% silicate melt. There are small variations in these proportions (by ±0.5 wt%) because the solubility of fluid components in the melts is not constant under the conditions studied.

High pressure experiments (1–2.5 GPa and 1400 °C) were carried out in the solid-media, high-pressure apparatus (Boyd and England, 1960) with 3/4″-diameter, tapered furnace assemblies (Kushiro, 1976). The experiments were terminated by turning off the power to the furnace, which results in an average cooling rate near 100 °C/s between experimental temperature and about 500 °C. Pressure precision is <0.05 GPa and accuracy ⩽0.1 GPa from calibration with the calcite-aragonite and quartz-coesite transitions and the melting point of NaCl (see Bohlen, 1984). Temperature was measured and controlled with Pt-$Pt_{90}Rh_{10}$ thermocouples with no pressure correction on the emf of the thermocouples. The precision is ±1 °C. Temperature accuracy is ⩽10 °C because of no correction for pressure on the thermocouple emf (Getting and Kennedy, 1970; Mao et al., 1971).

The hydrogen fugacity was buffered by the IW + H_2O equilibrium, $Fe + H_2O \leftrightharpoons FeO + H_2$, in order to maintain the reducing conditions needed to keep an essentially pure $CH_4 + H_2$ fluid phase in equilibrium with melt. A double-capsule technique for sample and buffer assemblage containment was employed (Eugster and Wones, 1962). With this method, the volatile-free silicate glass + tetrakis-silane + H_2O starting materials were loaded into an inner 3 mm-diameter by 4–5 mm long Pt capsule and welded shut. The sample-containing capsules were placed inside outer 5 mm-diameter by 10 mm Pt capsules together with the IW + H_2O hydrogen buffer material and welded shut. As the Pt wall of the inner capsule is permeable to H_2, the f_{H2} in the sample-containing, inner capsule is the same as that defined by the oxygen buffer + H_2O assemblage in the outer capsule (e.g., Eugster and Wones, 1962). The hydrogen fugacity of the IW + H_2O buffer was calculated from the dissociation constant and fugacity of H_2O (using SUPCRIT92) and the oxygen fugacity defined by the IW buffer assemblage at the high pressure and temperature of the experiments (from Huebner, 1971). The presence of both Fe metal and FeO (wüstite) after completion of an experiment was ascertained by reflected light petrographic microscopy by the significantly different reflectivity of metallic Fe and wüstite.

In order to determine the Na/Si of the experimental glasses, ~2 mg of crushed glasses that had been equilibrated with $CH_4 + H_2$ fluid at high pressure and temperature (see details below) were brought to temperatures above that of their liquidii and ambient pressure to form a melt and to release all volatile components dissolved during the initial high-pressure/-temperature melting. The samples were kept

at this condition for at least 1 h. The glasses formed by quenching of these latter melts were then analyzed for Na_2O and SiO_2 using a JEOL 8800 electron microprobe operating at 15 kV acceleration voltage and a beam current near 10 nAmp. To minimize potential problems with Na-loss from these Na-rich (~15 to ~30 wt% Na_2O) glasses during analysis, the analyses were conducted by rastering over ten to twenty 20 μm × 20 μm squares per sample. Glass compositions thus obtained are given in Table 1. The analyzed Na/Si ratio of the most sodic glasses, NS2 and N3S8, is slightly below nominal values (0.92 ± 0.04 and 0.69 ± 0.02 as compared with nominal values of 1.0 and 0.75, respectively). This small difference probably partially reflects a small loss of Na during electron microprobe analyses and party perhaps a small loss of Na during remelting of these volatile-bearing glasses under ambient pressure conditions.

The most SiO_2-rich melts (NS5, NS4 and, for the most part, N3S8) quenched to clear and colorless glasses with large spherical cavities (>10 μm across) reflecting the presence of a separate fluid phase during the high-pressure/-temperature experiments. There is no evidence for a separate C-phase (graphite or amorphous carbon). Exsolution of gas bubbles during quenching was a problem with quenched melts of NS2 composition and occasionally with N3S8. Bubbles formed by exsolution from melt during quenching are commonly of submicron size and unevenly distributed in the quenched glasses with textures similar to those observed in water-rich Na_2O–SiO_2 quenched glasses (e.g., Mysen and Cody, 2004). These NS2 glasses also contained large bubbles reflecting the presence of a separate fluid phase during the experiments. Exsolution of submicron-sized gas bubbles during quenching was also an occasional problem with N3S8 composition quenched melts. During micro Raman spectroscopic analysis of NS2 glasses (see details below) we attempted to avoid areas with quench bubbles. This may not always have been successful. Experimental data of NS2 melts are, therefore, subject to uncertainties that are difficult to evaluate.

The total carbon contents and $^{13}C/^{12}C$ of quenched glasses were analyzed with an Elemental Analyzer (EA) of CE Instruments, NC 2500 series interfaced with a gas chromatograph-combustion-isotope ratio mass spectrometer (GC/C/IRMS) (Finnigan MAT Delta$^+$ XL mass spectrometer interfaced with a Varian 3400 capillary GC). A Pora Bond Q capillary column (50 m × 0.32 mm ID) at 35 °C with a helium carrier gas was used. The samples were weighed into 3.5 × 5 mm ultra clean silver capsules. After weighing, the capsules were sealed and introduced in to the EA via an auto-sampler. Within the EA, each sample was combusted with ultra pure oxygen at 1020 °C in a quartz oxidation column containing chromium (III) oxide and silvered cobalt (II, III) oxide. The resulting gas was mixed with zero-grade helium carrier gas. CO_2 was separated using a Haysep Q GC column (2 m × 2.1 mm ID) at 80 °C prior to entering a Finnigan Conflo II interface. All isotope values are reported in delta notation ($\delta^{13}C$),

$$\delta^{13}C = ((R_{sample}/R_{standard}) - 1) \times 1000 \quad (2)$$

where R_{sample} and $R_{standard}$ are the $^{13}C/^{12}C$ of the sample and the international standard (Vienna PeeDee Belemnite; Craig, 1957), respectively. The analytical precision associated with stable carbon isotope analysis by this method for standard compounds (e.g., acetanilide and a well characterized sediment) is ±0.3‰.

Glasses were crushed to ~10–20 μm grain size before analysis in part in order to ensure that bubbles that may have contained fluid from high-pressure experiment released all inclusion content. The powdered glass was heated at 50 °C for 6 h prior to carbon elemental and isotopic analysis in order to remove water because these Na-rich glasses are quite hydroscopic. Duplicate analyses of several splits of individual experimental glasses were always within ±0.4‰ of each other or less.

Hydrogen in the glasses is partly from methane dissolved in the samples, partly from OH groups in the glasses formed by interaction of methane or hydrogen, or both, with silicate melts (see below), and partly from H_2O adsorbed (and absorbed?). Adsorbed or absorbed water is an increasing problem the more sodic the glasses. This hygroscopic behavior makes hydrogen analyses and unreliable indicator of hydrogen actually dissolved in the quenched melts.

The species in the fluid phase quenched from that which coexisted with melts during experiments were identified after gas extraction from the capsules (via a capsule puncturing procedure within an evacuated vial) before the glass was recovered for chemical, isotopic, and spectroscopic analyses. A Shimadzu G8 gas chromatograph equipped with a thermal conductivity detector (GC/TCD) was used for species identification. Uncertainties associated with possible back reaction of the fluid during temperature quenching (including possible interaction with the melt) cannot be evaluated. Quantitative analyses of the gas phase are, therefore, considered unreliable and only qualitative speciation information will be considered.

The structure of quenched methane-saturated melts was characterized with Raman and NMR spectroscopy. The Raman spectrometers were Witec SMOW α and JASCO NRS-3100 confocal microRaman systems with 8–10 mW laser power of the 532 nm frequency-doubled line from a Nd-YAG laser for sample excitation. A 100× objective lens (N.A. = 0.7) was used for all measurements. With this setup the laser beam diameter on the sample is less than 1 μm, with a penetration depth of 2–3 μm into the samples. The position of the laser during the Raman measurements was monitored optically to minimize or eliminate interference with signals from the glass from signals of fluid that existed

Table 1
Composition of volatile-free glasses (wt%).

	NS2	N3S8	N4	NS5
SiO_2	67.13 ± 0.56	72.48 ± 0.26	77.28 ± 0.25	83.11 ± 0.22
Na_2O	31.87 ± 1.17	25.57 ± 0.39	22.04 ± 0.26	15.23 ± 0.91
Na/Si	0.92 ± 0.04	0.69 ± 0.02	0.55 ± 0.02	0.36 ± 0.02
Nominal Na/Si	1.00	0.75	0.50	0.40

in some of the most sodic samples (NS2 composition and some glasses for N3S8). Uncertainty in laser beam position is 2–3 μm.

Hydrogen-1 MAS NMR data were recorded with a Chemagnetics CMX Infinity 300 Solid State NMR. The static field strength of the magnet is 7.05 T. The Larmor frequency of ^{1}H at this field is 300 MHz. The spectra were acquired from 10–20 μm grain size glass powder contained in 5 mm OD zirconia rotors and a Chemagnetics double-resonance probe. Background of the ^{1}H signal was suppressed using the pulse program of Cory and Ritchey (1988) with ^{1}H excitation pulses ($\pi/2$) of 4 μs, a spectral width of 200 KHz, and a 5 s pulse delay. A total of 6400 acquisitions were acquired per sample at a MAS speed of 12 KHz. The total acquisition time was 5.12 ms (1024 points). The resultant FID was zero filled out to 8192 points before Fourier Transformation. The ^{1}H MAS spectra were referenced to the proton resonance of TMS.

3. RESULTS

Experimental results are summarized in Table 2. Solubility is reported as total C content and the $\delta^{13}C$ relative to Vienna PeeDee Belemnite (Craig, 1957).

Table 2
Experimental results.

Composition	Pressure (GPa)	Time (min)	Total C (wt%)	$\delta^{13}C$[a] (‰)
NS5	1	30	n.d.[b]	−21.9
NS5	1.5	5	0.12	−17.2
NS5	1.5	15	0.15	−17.6
NS5	1.5	30	0.12	−17.2
NS5	1.5	60	0.13	−18.1
NS5	2	30	0.19	−19.1
NS5	2.5	30	0.18	−17.3
Average			0.15 ± 0.03	−17.8 ± 0.7
NS4	1	30	0.15	−24.4
NS4	1.5	30	0.16	−22.4
NS4	2	30	0.3	−22.7
NS4	2.5	30	0.2	−22.2
Average			0.20 ± 0.07	−22.9 ± 1
N3S8	1	30	0.14	−21
N3S8	1.5	30	n.d.	−26.2
N3S8	2	30	0.24	−29.4
N3S8	2.5	30	0.27	−29.3
Average			0.22 ± 0.07	−26.5 ± 3.9
NS2	1	30	n.d.	−36.4
NS2	1.5	30	0.21	−32.1
NS2	2	30	0.43	−25.2
NS2	2.5	30	n.d.	−33.4
Average			0.32 ± 0.16	−31.8 ± 4.7

[a] Tetrakis-silane value: −49.9‰.
[b] Not determined.

3.1. Equilibrium considerations

Results of a time study of carbon concentration and $\delta^{13}C$ in melts at 1400 °C and 1.5 GPa with NS5 composition melt at 5, 15, 30, and 60 min experimental duration are shown in Table 2. The NS5 composition was chosen because it is the most viscous of those used here (Bockris et al., 1955) and, therefore, likely would have the lowest diffusivity of the C-bearing species in the melts.

The carbon contents were insensitive to run duration in all experiments. The $\delta^{13}C$ reaches a constant value after 15 min. Fifteen minutes are, therefore, considered the minimum time necessary for chemical and isotopic equilibration between the silicate melt and the coexisting ($CH_4 + H_2$) gas in the experiments. This duration is not unreasonable because total transport distances needed for equilibration between gas and melt in the experimental setup are <50 μm. Although diffusion coefficients for CH_4 in silicate melts is not well known, by using diffusion coefficients for H_2O in silicate melts of similar degree of melt polymerization as an analog (e.g., Chekhmir et al., 1988; Zhang et al., 1991; Doremus, 1995; Behrens and Nowak, 1997), we conclude that at 1400 °C, transport distances of CH_4 would be on the order of several hundred μm after 15 min. We, therefore, conclude that the 30-min duration of all experiments was sufficient to reach equilibrium.

3.2. Solubility

The total carbon content, calculated as CH_4, of melts in equilibrium with ($CH_4 + H_2$) fluid as a function of their Na/Si at 1400 °C is shown in Fig. 1. We will refer to this as methane solubility even though the (C..H) complexes in the melts may not be in the form of CH_4 (see also below).

Methane solubility is a simple and positive function of Na/Si (=NBO/Si—nonbridging oxygen per silicon) and more than doubles in the NBO/Si-range of melts from NS5 to NS2 (Fig. 1). In this respect the methane solubility resembles that solubility behavior of oxidized carbon such as CO_2, which is also positively correlated with NBO/Si of melt (e.g., Holloway et al., 1976; Brooker et al., 2001).

The C content of each melt in Fig. 1 is the average value from 1, 1.5, 2, and 2.5 GPa experiments because there is no discernible effect of pressure of the C solubility (Table 2). The lack of pressure effect on methane solubility may not be surprising because at 1400 °C, the fugacity of H_2, f_{H2}, defined by the redox equilibrium, $Fe + H_2O = FeO + H_2$ ($IW + H_2O$), changes only by ~15% between 1 and 2.5 GPa (Mysen et al., 2008).

Published experimental data on carbon solubility in silicate melts under conditions comparable those of the present experiments are scarce. Kadik et al. (2004) reported 0.16 wt% C in tholeiitic melts at 3.7 GPa and 1520–1600 °C under conditions suggested to be near IW-2.3. Holloway and Jakobsson (1986) reported C contents on the order of 0.2 wt% in tholeiite melt in the 1–2 GPa pressure range under redox conditions resembling those of the present experiments. Direct comparison with the present experiments is not, however, possible because information on

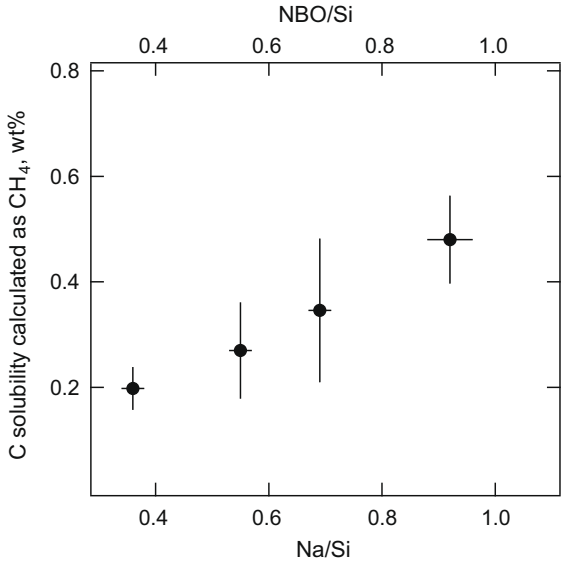

Fig. 1. Solubility of carbon (calculated as wt% CH_4) in Na_2O—SiO_2 melts as a function of their Na/Si (and NBO/Si). The individual C concentrations are given in Table 2 The error bars are the standard errors ($\pm 1\sigma$) of the average of solubility data at 1, 1.5, 2, and 2.5 GPa and replicate analyses for each of the compositions.

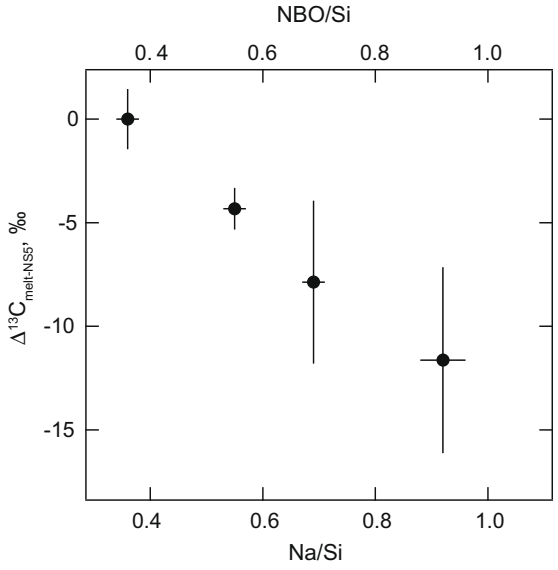

Fig. 2. $\delta^{13}C$ difference and Na_2O—SiO_2 melts as a function of their Na/Si (and NBO/Si). The difference is calculated relative to the value for NS5 composition melts. The individual $\delta^{13}C$ values are given in Table 2. The carbon isotope ratio of the C-source in all experiments, tetrakis-silane, is −49.9‰. The error bars are the standard errors ($\pm 1\sigma$) of the average of solubility data at 1, 1.5, 2, and 2.5 GPa and replicate analyses for each of the compositions.

possible pressure, temperature, and composition dependence is not available.

3.3. Carbon isotopes

The $\delta^{13}C$ of the glasses quenched from melt in equilibrium with ($CH_4 + H_2$) fluid are given in Table 2. The source of methane in all experiments (tetrakis-silane) was the same with $\delta^{13}C = -49.9‰$.

The change with Na/Si of $\delta^{13}C$ of these quenched melts are shown relative to the $\delta^{13}C$ value for NS5 in Fig. 2. For each melt composition, average values of results from experiments in the entire pressure range (1–2.5 GPa) are used because $\delta^{13}C$ does not appear significantly pressure-dependent (Table 2).

The C isotope fractionation between that of the starting material and the silicate glasses was large, ranging from +18 to 30‰. In addition to this isotopic fractionation, there is a ~14‰ change in $\delta^{13}C$ in melts coexisting with ($CH_4 + H_2$) fluid as a function of melt composition (Fig. 2). These carbon isotopic variations are not likely attributable to variables in the experimental protocol because proportion of coexisting fluid and melt in all experiments was nearly constant ($5 \pm 0.5\%$ gas and $95 \pm 0.5\%$ melt) and the CH_4/H_2 of the fluid also the same because the f_{H2} is nearly constant in all the experiments.

3.4. Spectroscopy of C-bearing melts

Solution mechanisms of reduced C—O—H volatile species in melts were evaluated with Raman and ^1H MAS NMR spectroscopy. The Raman spectra were used to characterize C—O, C—H, H—H, and O—H bonding and linkages to and bonding within the silicate melt structure (Figs. 3–6). The ^1H MAS NMR spectra provide additional constraints on the nature of H-bearing complexes (Fig. 7).

3.4.1. Raman spectra in the 250–1400 cm^{-1} frequency range

The frequency region between about 250 and 1400 cm^{-1} encompasses that of 1st-order Si—O Raman scattering. Raman bands assignable to Si—C and Si—CH_3 vibrations would also occur in this frequency range (e.g., Wright and Hunter, 1947; Burton et al., 1998).

The Raman spectra of quenched melts in this spectral region are dominated by major intensity maxima near 500–600 and 1100 cm^{-1} (Fig. 3). These spectra differ from those of volatile-free melts in that width of the peaks with maxima increases in spectra of the ($CH_4 + H_2$)-saturated quenched melts (e.g., Fig. 4).

These spectroscopic differences can be enhanced by computing difference spectra where spectra of volatile-free quenched melts are subtracted from those of ($CH_4 + H_2$)-saturated quenched melts. Two examples, from NS2 and NS4 compositions, are shown in Fig. 5. There is a clear negative intensity difference increase near and slightly above 500 cm^{-1}, a minor negative intensity difference near 800 cm^{-1} and a pronounced negative intensity increase at and above about 1100 cm^{-1}. Positive intensity differences occur near 600 cm^{-1}, 950 cm^{-1} and 1000 cm^{-1} (Fig. 5). The extent of these intensity changes depends on melt composition and are comparatively insensitive to pressure (Fig. 5 and Table 2).

3.4.2. Raman spectra in the 1400–4200 cm^{-1} frequency range

The upper panels in Figs. 3 and 4 show the spectra in the range from about 250–3850 cm^{-1} with an expansion of the

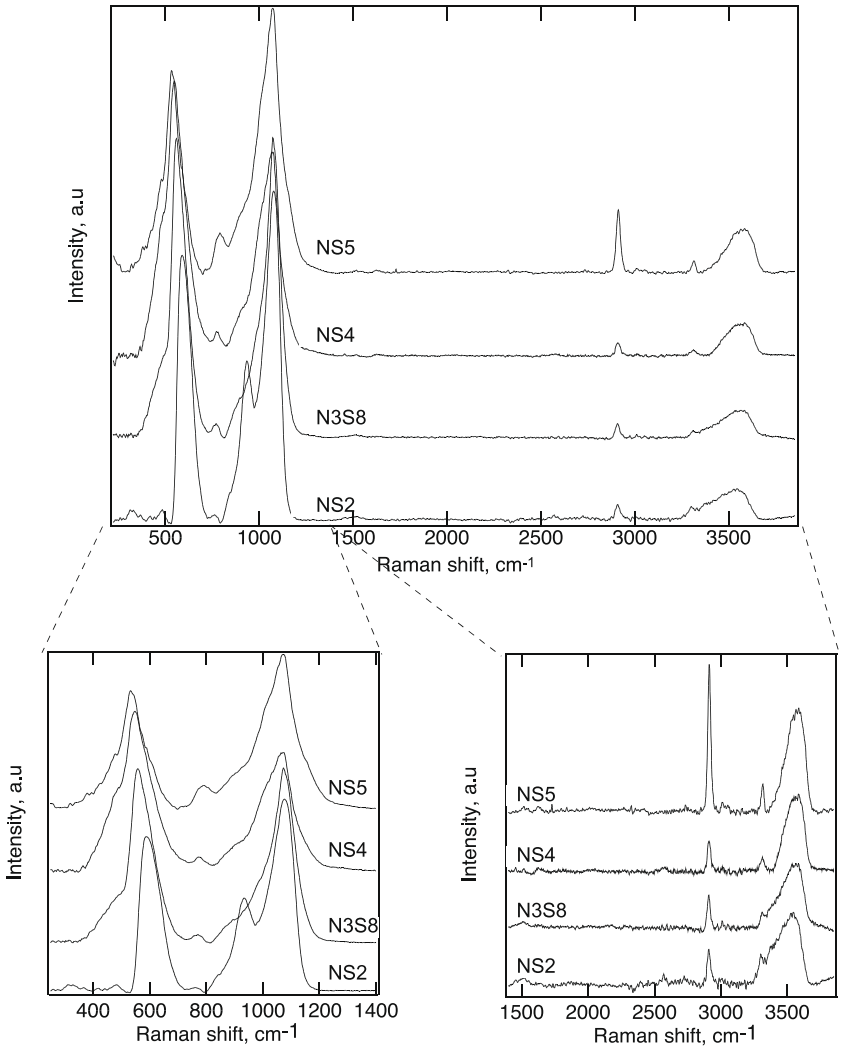

Fig. 3. Raman spectra of quenched melts with compositions as indicated on individual spectra. The melts were equilibrated at 1.5 GPa. Expanded portions of selected portions of the frequency range are shown in the lower panels.

1400–3850 cm^{-1} frequency range in the lower right panels. The 1400–3850 cm^{-1} frequency range is that within which vibrations from Si—O, C—O, C—H, and O—H bonds would be expected. In order to extend the spectral range to include that where H—H vibrations from molecular H_2 would be expected, a separate set of spectra extending to 4250 cm^{-1} were recorded. Examples from the N3S8 quenched melt composition are shown in Fig. 6.

There are 3 narrow peaks (FWHH ~15–25 cm^{-1}) near 2920, 3310, and 4130 cm^{-1}, and a broad asymmetric maximum near 3600 cm^{-1}. There may also be one or two very weak peaks near 1520 and 1620 cm^{-1}, respectively. For the most polymerized melts (NS4 and NS5 composition), there are also one or two weak peaks near 3000 and 3050 cm^{-1}. These latter two features are enhanced in the inserts in the lower right panel of Fig. 5B.

There appear no be no available Raman spectra of methane-bearing silicate melts and glasses with which to compare the present data. However, we note that a broad asymmetric peak is always present in spectra of water-bearing glasses and melts (e.g., Stolen and Walrafen, 1976; McMillan and Remmele, 1986; Yamashita et al., 2007). A strong and sharp Raman band near 2900 cm^{-1} is characteristic of spectra from methane-bearing fluid inclusions and from methane chlatrates (e.g., Pasteris et al., 1990; Murphy and Roberts, 1995; Dubessy et al., 2001). A peak near 4250 cm^{-1} is a characteristic feature of hydrogen-bearing melts and chlatrates (e.g., Luth et al., 1987; Murphy and Roberts, 1995).

3.4.3. Hydrogen-1 MAS NMR spectra

The NMR spectra are shown in Fig. 7 with narrow peaks near 1.3, 1.5, 2.4, 4.3, and 5.4 ppm and a much broader peak centered near 15 ppm. A similar broad peak is observed in the spectrum of NS4 glass with 5.5 wt% H_2O dissolved, but without C-bearing components in solution. Similar spectral features are common in ^1H MAS NMR spectra of hydrous glasses (e.g., Kohn et al., 1989; Cody et al., 2005). To the best of our knowledge, ^1H MAS NMR spectra of silicate glasses from melts equili-

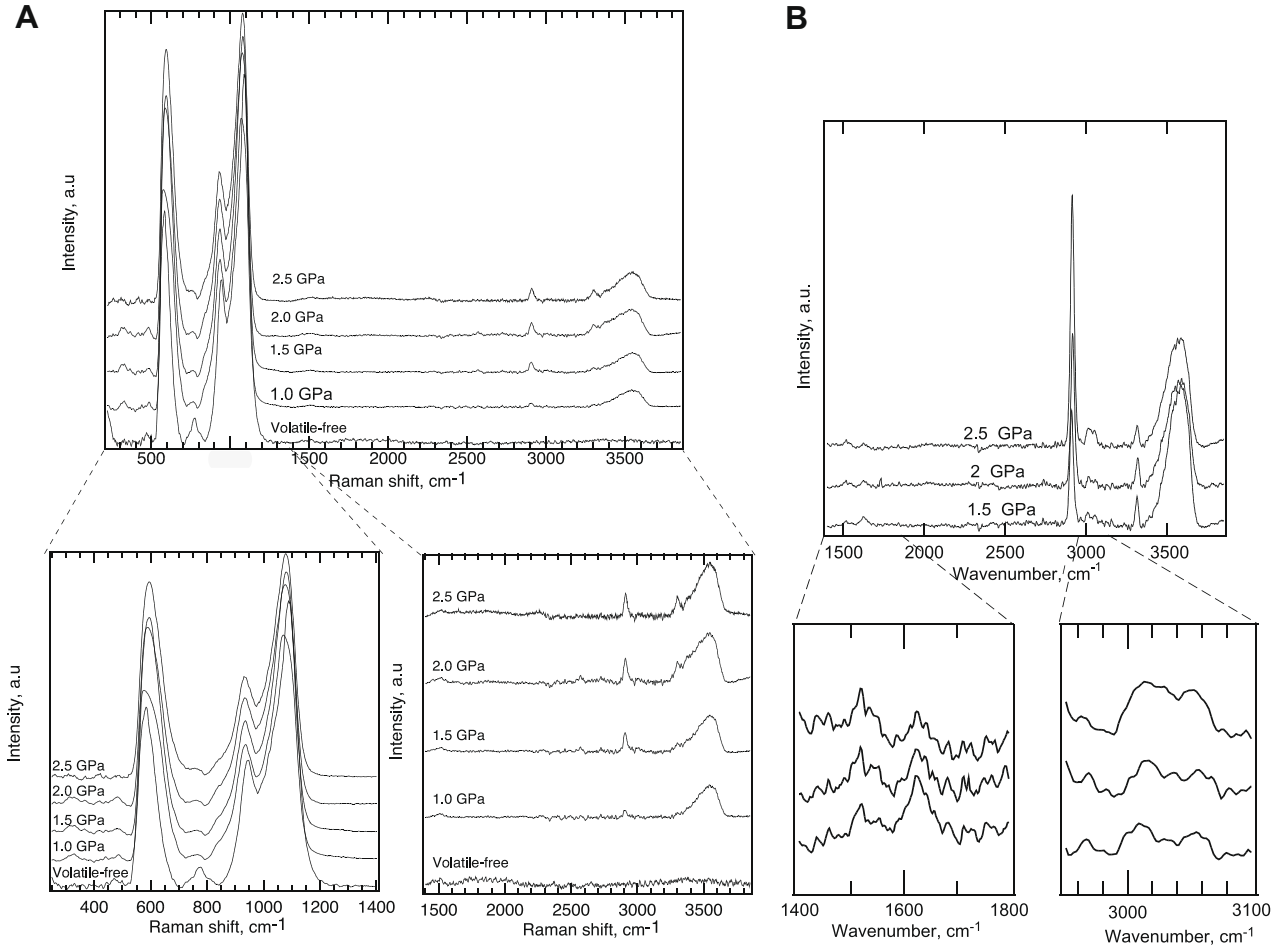

Fig. 4. Raman spectra of quenched melts as a function of pressure. (A) Quenched NS2 composition melts. (B) Quenched NS5 composition melts. Expanded portions of selected portions of the frequency range are shown in the lower panels.

brated with CH_4-rich fluids at high pressure and temperature with which to compare these spectra have not been reported.

4. DISCUSSION

4.1. Band assignments and structural interpretations

4.1.1. NMR spectroscopy

The peaks near 1.3, 1.5, 2.4, 4.3, and 5.4 ppm in the ^{1}H MAS NMR spectrum of quenched NS4 + CH_4 melt are assigned to protons in (C..H)-containing complexes (Pretsch et al., 2000), whereas the broad peak centered near 15 ppm and the broad intensity beneath the sharper peaks in the 7–0 ppm range are assigned to proton resonances in OH groups (e.g., Kohn et al., 1989; Cody et al., 2005). These features are further demonstrated with the ^{1}H MAS NMR spectrum of hydrous (~5.5 wt% H_2O) NS4 melt composition where only broad peaks near 7 and 15 ppm can be seen (Fig. 7).

From the reference data base of Pretsch et al. (2000) of ^{1}H NMR spectra of organic compounds, the peaks at 2.4, 1.5, and 1.3 ppm may be assigned to resonance in ^{1}H in molecules that include C—H bonding and weak peaks near 5.4 and 4.3 ppm possibly to ^{1}H resonance in metoxy groups (—O—C—H). However, when using the data base of Pretsch et al. (2000) to aid in assignments of ^{1}H NMR spectra from silicate melts it should be remembered that the exact frequencies likely depend on the local environment near the proton analogous to that observed and predicted for gas molecules in chlatrates (e.g., Florusse et al., 2004; Alavi et al., 2005). Frequency variations of peaks assigned to H-bearing complexes in these glasses could, therefore, reflect interaction between the H-containing components and the silicate.

A likely assignment of the 2.4 ppm peak is to proton resonance in C≡C—H-containing complexes. Those near 1.5 and 1.3 ppm could be due to H in CH_3 complexes, to CH_2, CH_4, or perhaps simply H_2 because the ^{1}H shift is very sensitive to environment near the ^{1}H nucleus. For example, local environmental variations have been reported to cause several ppm shifts in the ^{1}H resonance of H_2 in chlatrates as compared with the shift of isolated H_2 molecules (Florusse et al., 2004; Strobel et al., 2006). Even greater frequency changes can be caused by hydrogen bonding (e.g., Cody et al., 2005). The assignments of the ^{1}H MAS

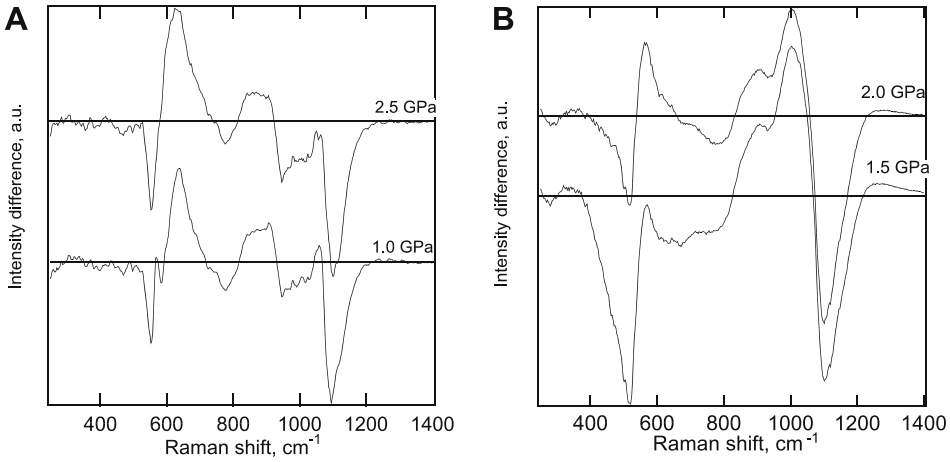

Fig. 5. Difference Raman spectra of quenched melts where spectra of volatile-free quenched melts subtracted from spectra of quenched melts equilibrated at pressures as indicated on individual spectra. (A) NS2 composition quenched melts. (B) NS4 composition quenched melts.

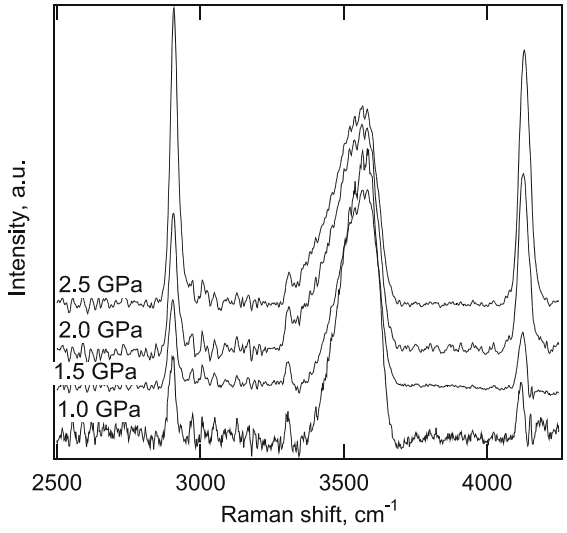

Fig. 6. Example (for composition N3S8) of Raman spectra as a function of pressure in the frequency range between 2500 and 4250 cm^{-1}.

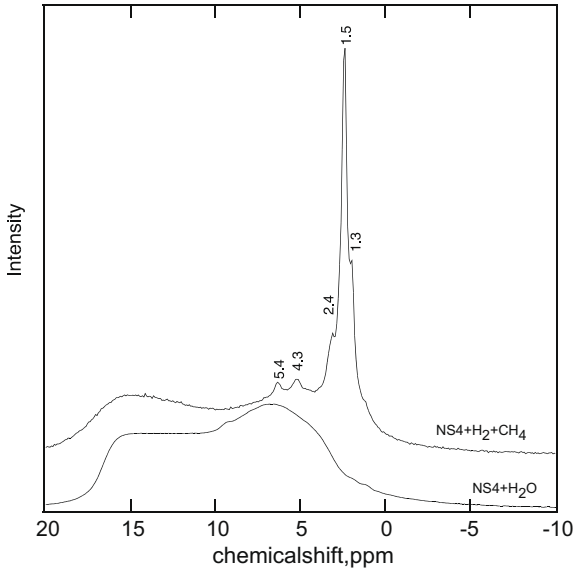

Fig. 7. Hydrogen-1 MAS NMR spectra of $Na_2Si_4O_9$ (NS4) with 5.5 wt% H_2O in solution ($NS_4 + H_2O$—lower spectrum), ($H_2 + CH_4$)-saturated ($NS4 + H_2 + CH_4$—upper spectrum).

NMR spectrum are not, therefore, certain and require substantiation with examination by other spectroscopic methods. Raman spectroscopy is used here for this purpose.

4.1.2. Raman spectroscopy

The interpretation of the Raman spectra in the 250–1400 cm^{-1} range was aided by difference spectra (Fig. 5). Before discussing assignments and interpretations of such spectra, uncertainties and limitations associated with the use of difference spectra must be kept in mind. We note in particular that if the abundance of different structural entities in the melts varies at the same time, it may be difficult to extract the exact frequencies at which intensity changes actually occur because of changing overlap of bands assigned to individual vibrations. Furthermore, intensity variations in the difference spectra represent small differences between large numbers, and are, therefore, associated with significant relative uncertainties. Finally, Raman cross sections of different vibrations are not the same, making quantification of changes in species abundance on this basis alone uncertain. Intensity changes are, nevertheless, correlated with abundance.

With these limitations in mind, qualitative interpretation of the Raman intensities in the 250–1400 cm^{-1} frequency range in terms of silicate glass and melt structure is nevertheless possible thanks to the numerous previous NMR and Raman spectroscopic studies of well constrained binary silicates and ternary aluminosilicates (see chapters 7 and 9 of Mysen and Richet, 2005, for review of those data).

The major positive component in the Raman difference spectra is in the 900–1000 cm^{-1} frequency region (Fig. 5) and is attributed to stretch vibrations of (Si)—O^- bonds,

where the nonbridging oxygen, O^-, most probably is in Q^1 and Q^2 units (Brawer and White, 1975, 1977; Furukawa et al., 1981; McMillan, 1984; Mysen and Frantz, 1992; Mysen, 1997). That interpretation is substantiated with concurrent intensity increase between ~590 and ~650 cm^{-1}. Raman bands in this frequency region are assigned to Si—O—Si bending vibrations in Q^3, Q^2, and Q^1 structural (e.g., Furukawa et al., 1981; Kubicki et al., 1992), which, of course, also contain nonbridging oxygens. However, bands that can be assigned to Si—OH vibrations also occur in the 950–980 cm^{-1} frequency range (e.g., Stolen and Walrafen, 1976; McMillan and Remmele, 1986; McMillan et al., 1993; Sykes and Kubicki, 1993). The presence of Si—OH bonds in silicate melts does not, however, result in Raman bands in the 590–650 cm^{-1} frequency range. This conclusion does not, however, rule out that a portion of the 900–1000 cm^{-1} intensity being because of Si—OH groups in the melts.

The main negative intensity differences are near or slightly below 500 cm^{-1} and above 1100 cm^{-1} (Fig. 5). A band near 1150 cm^{-1} is commonly assigned to Si—O stretching in fully polymerized Q^4 structural units (McMillan et al., 1982; Seifert et al., 1982; Matson et al., 1986; McMillan and Wolf, 1995; Neuville and Mysen, 1996). A band near 450 cm^{-1} is assigned to Si—O rocking motion in fully polymerized Q^4 units (McMillan et al., 1982; McMillan and Wolf, 1995). Thus, the decreasing intensities in the ~500 and >1100 cm^{-1} likely reflect decreasing abundance of Q^4 structural units in the glasses. Decreased abundance of Q^4 units is consistent with melt depolymerization.

Bonding of Si to C or CH_3 groups would be detectable as bands assignable to Si—C and Si—CH_3 stretching in the 800–900 cm^{-1} and 1250–1300 cm^{-1} frequency ranges, respectively (Wright and Hunter, 1947; Burton et al., 1998). There is no additional Raman intensity in these frequency regions in any of the Raman spectra of ($CH_4 + H_2$)-saturated melts. Thus, we have no evidence suggesting bonding of Si directly to either C or CH_3.

The sharp Raman band near 2920 cm^{-1} (Figs. 4 and 5) can be assigned to C—H stretch vibrations in CH_4, CH_3, or CH_2 groups (Socrates, 2001). Its frequency is similar to that of CH_4 (methane) as observed, for example, in Raman spectra of CH_4-containing fluid inclusions (e.g., Seitz et al., 1987; Dubessy et al., 1999, 2001) suggesting that this band most likely should be assigned to C—H stretching in CH_4 groups. In light of this interpretation it seems reasonable that at least one of the intense peaks in the 1.3–1.5 ppm range of the ^1H MAS NMR spectra (Fig. 7) should be assigned to ^1H resonance in CH_4 molecules in the melts.

The relatively sharp band near 3310 cm^{-1} can be assigned to C—H stretching in an alkyne group, —C≡C—H. For comparison, Raman bands that can be assigned to C—H stretching in groups with double- and single-bonded carbon, —C=CH and —C—CH, occur at significantly lower (>100 cm^{-1}) Raman frequency than the observed 3310 cm^{-1} frequency (Socrates, 2001). It is unlikely, therefore, that groups with double- or single-bonded carbon play important roles in the melts. The ^1H MAS NMR 2.4 ppm peak in Fig. 7 is also consistent with proton nuclei in such complexes containing triple-bonded C (e.g., Pretsch et al., 2000).

The weak Raman bands between 3000 and 3050 cm^{-1} in NS5 and NS4 composition melts (see insert in Fig. 4B for an example) may be assigned to C—H stretch vibrations in —O—CH_3 groups (Socrates, 2001), which is also consistent ^1H NMR intensity in the 4–5 ppm range (Fig. 7; see, Pretsch et al., 2000). Whether these latter bands can be seen only in spectra of the most polymerized samples (NS4 and NS5) because of spectral sensitivity or whether O—CH_3 bonds are not present in spectra of less polymerized methane-saturated melts cannot be ascertained.

The narrow and strong Raman band near 4130 cm^{-1} (Fig. 6) is at nearly identical frequency and has similar FWHH to that of H—H vibration in molecular H_2 dissolved in H_2-saturated $NaAlSi_3O_8$ composition quenched melts (e.g., Luth et al., 1987). This assignment is retained for the spectra of the ($H_2 + CH_4$)-saturated melts studied here. It follows from this interpretation and proton NMR data for hydrogen chlatrate (e.g., Alavi et al., 2005) that one of the peaks between 1.3 and 1.5 ppm in the ^1H MAS NMR spectrum (Fig. 7) could be assigned to molecular H_2.

Finally, the broad (FWHH ~200 cm^{-1}) asymmetric Raman band with a maximum near 3600 cm^{-1} is assigned to O—H stretching in OH groups (whether bonded to metal cations or protons, as in H_2O). The very week, but commonly observed broad band near 1600 cm^{-1} (e.g., insert in Fig. 4B) can then be assigned H—O—H bending in H_2O molecules.

4.2. Molecular species and (C..H) complexes

Additional information on the solution mechanisms of C—O—H volatiles in the melts may be obtained by curve-fitting of the Raman spectra. An example from the most depolymerized sample (NS2) is shown in Fig. 8.

4.2.1. Molecular species in solution or from exsolution?

Whether CH_4 and H_2 molecules are dissolved in the melts or exist in submicroscopic inclusions may be evaluated by comparing frequencies and full Raman line widths at half height (FWHH) as well as the response to pressure of the 2920 and 4130 cm^{-1} Raman bands from the glasses with those reported for pure H_2 and CH_4.

The Raman frequencies of the peak maxima differ from those of the pure gases. For pure methane, at ambient conditions the frequency of C—H vibrations in gaseous CH_4 is 2918 cm^{-1} (e.g., Pasteris et al., 1990), whereas that of hydrogen is near 4150 cm^{-1} (e.g., Nakamoto, 1978). The respective frequencies of both bands for the quenched melts are up to several tens of cm^{-1} lower than for gaseous CH_4 and H_2 and depend on pressure (see Fig. 9A and C). Such lower frequencies suggest interaction of CH_4 and H_2 molecules with the silicate melt solvent, which would weaken C—H and H—H bonds in dissolved CH_4 and H_2 molecules compared with gaseous CH_4 and H_2 molecules. Weakened C—H and H—H bonding is also consistent with the ^1H NMR data where the frequency shifts of peaks assigned to proton resonance in H_2 and CH_4 suggest some deshielding of the hydrogen nucleus. Deshielding could be the result of interaction between CH_4 and H_2 molecules and the silicate melt in which these molecules are dissolved.

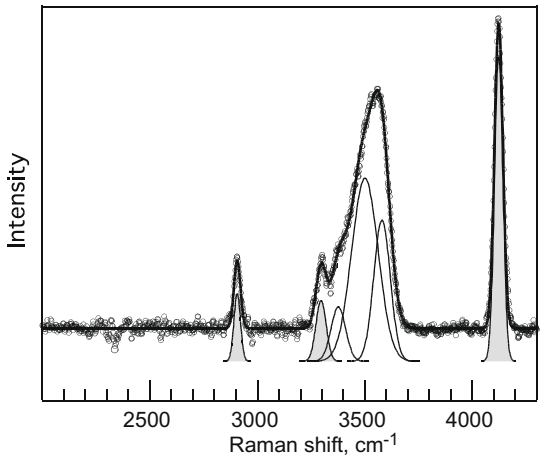

Fig. 8. Example of curve-fitted Raman spectrum from NS2 composition quenched after equilibration at 2.5 GPa.

The FWHH of the 2920 and 4130 cm^{-1} bands in gaseous H_2 and CH_4 typically is on the order of 5–10 cm^{-1} at ambient temperature (e.g., Nakamoto, 1978; Pasteris et al., 1990). In the spectra in Figs. 3, 4 and 6, the FWHH-values are larger and range from about 15 cm^{-1} to in some instances more than 25 cm^{-1}. The FWHH-values are also positively correlated with pressure (Fig. 9B and D) suggesting perhaps distortion of local symmetry.

The FWHH-values of the 4130 cm^{-1} peak (Fig. 9D) (assigned to vibrations in molecular H_2) are also similar to those reported for dissolved H_2 in other high-pressure melts (Luth et al., 1987). To our knowledge Raman data for molecular CH_4 in silicate melts have not been reported previously. It is noted, however, the FWHH of ~2920 cm^{-1} Raman band is similar to that of CH_4 in spectra of methane chlatrates (e.g., Pasteris, 1987; Murphy and Roberts, 1995), where there is interaction between the CH_4 molecule and the chlatrate host.

It seems reasonable to conclude, therefore, that the significantly broader Raman bands, their pressure dependence, their frequencies, and the pressure-dependent frequencies indicate perturbations of C—H and H—H bonds in CH_4 and H_2 molecules that would be expected with CH_4 and H_2 molecules dissolved in melts suggesting interaction between the CH_4 and H_2 molecules and the silicate melts. This would not be expected if CH_4 and H_2 exist in a separate fluid phase whether as micron- or submicron-sized bubbles.

Most likely, these CH_4 and H_2 molecules occupy cavities in the silicate melt structure in a manner perhaps similar to

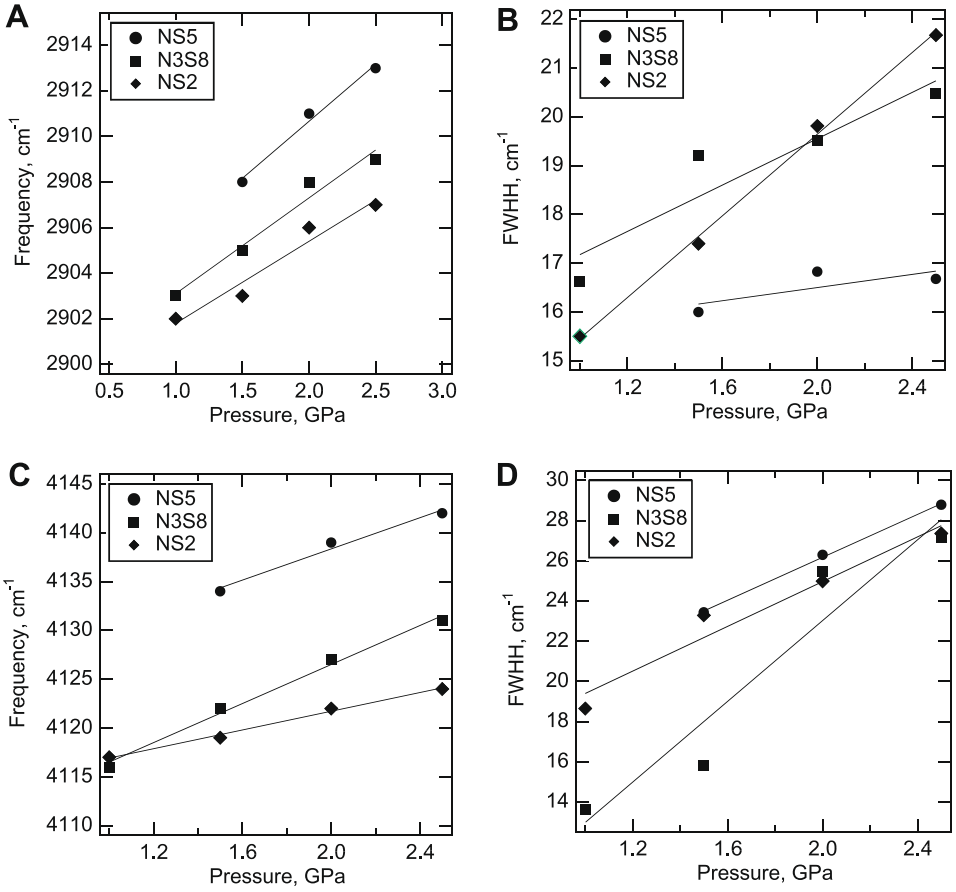

Fig. 9. Frequency and full width at half height (FWHH) of the band near 2920 cm^{-1} (A and B) and that near 4130 cm^{-1} (C and D), for the compositions indicated.

that suggested for noble gases and molecular N_2, CO_2, and H_2O (see, for example, Shelby, 1976; Fine and Stolper, 1986; Jambon et al., 1986; Carroll and Stolper, 1991; Carroll and Webster, 1994; Libourel et al., 2003). In fact, equilibria that involve molecular species and complexing with silicate melts commonly form the basis for models of solubility and solution mechanisms of volatile components in silicate melts at high pressure and temperature (e.g., Hodges, 1974; Stolper, 1982; Fine and Stolper, 1986; Kohn et al., 1991; Kohn, 2000; Brooker et al., 2001).

4.2.2. Silicate-C—O—H complexes in melts

The interpretation of the NMR and Raman spectra suggests a significant a significant role of (C≡C—H)-containing and a lesser role of (O—CH_3)-containing groups or complexes in the melts. Hydrogen is also dissolved as a part of OH groups. The intensity variations of Raman bands assigned to Si—O vibrations (Fig. 5) indicate that formation of those complexes leads to depolymerization of the silicate structure. There is no spectroscopic evidence for Si—C or Si—CH_3 bonding in the melts.

Ratios of integrated areas of Raman bands assigned to vibrations in particular bonds are positively correlated with the abundance of the species within which the bonding occurs. Changes of the integrated area ratios, A_{2920}/A_{3310}, and A_{3310}/A_{4130}, are in response, for example, to variations in abundance ratios, CH_4/C≡C—H (A_{2920}/A_{3310}) and C≡C—H/H_2 (A_{3310}/A_{4130}) (Fig. 10). Here, the notation, C≡C—H, is meant to indicate the presence of an alkyne group. However, the exact nature of this group (e.g., stoichiometry) cannot be established from the present data and proposed solution mechanisms are, therefore, necessarily qualitative and often schematic.

The relative abundance of the C—O—H-containing complexes is a systematic function of Na/Si of the melts (Fig. 10). The decreasing CH_4/H_2 with NBO/Si (Fig. 10A) probably is in response to decreasing availability of structural cavities in which to accommodate the molecular species where that larger molecular species (CH_4) and more sensitive to the cavity availability than smaller molecules (H_2). Such a size-dependent solubility trend is similar to that of noble gases in silicate melts (for review of relevant noble gas solubility data, see Carroll and Webster, 1994; Mysen and Richet, 2005, ch. 16). There is also decreasing CH_4/C≡C—H (A_{2920}/A_{3310}) with decreasing melt polymerization (increasing NBO/Si) (Fig. 10B), which leads to the suggestion that the C≡C—H complex forms bonds with nonbridging oxygen rather than breaking bridging oxygen bonds in silicate melts. Such a solution mechanism can be illustrated schematically as follows:

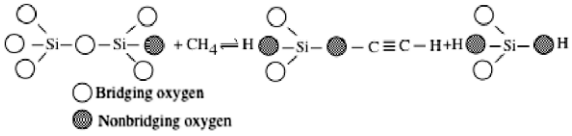

(3)

In this expression, C≡C—H forms bonds with nonbridging oxygen. The excess hydrogen released from CH_4 from such a reaction reacts with oxygen in the melts to form of Si—OH bonds. Note, however, that Eq. (3) is not meant to be a complete representation of the equilibrium between dissolved methane and silicate melts. It merely is meant to illustrate the central structural principles. Current data are insufficient to derive a complete and quantitative reaction mechanism.

5. APPLICATIONS

5.1. Solution mechanisms and liquidus phase relations

The solution mechanism summarized schematically in Eq. (3) implies depolymerization of the silicate melts structure. Depolymerization of silicate melts leads to decreasing silica activity. Depolymerization is consistent, therefore, with published data on liquidus phase relations of silicate systems in the presence of CH_4-rich fluid (Eggler and Baker, 1982; Taylor and Green, 1987) where the liquidus volume of forsterite expands relative to those of more polymerized silicate minerals such as pyroxene and garnet (see also Fig. 11). A forsterite liquidus volume expansion implies decreasing activity of silica (e.g., Carmichael et al., 1970; Kushiro, 1975; Ryerson, 1985).

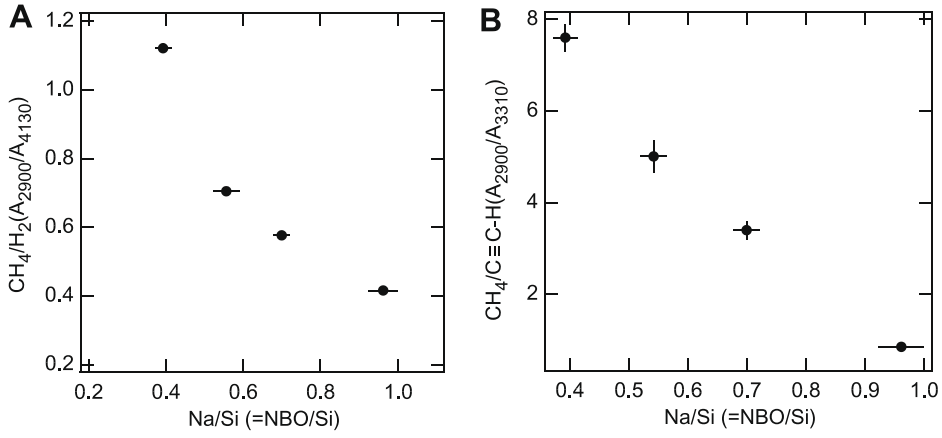

Fig. 10. Area ratios of Raman bands assigned to CH_4 (2920 cm^{-1} band), C≡C—H (3310 cm^{-1} band), and H_2 (4130 cm^{-1} band) as a function of Na/Si of the quenched melts. For volatile-free melts, Na/Si = NBO/Si (shown in parentheses).

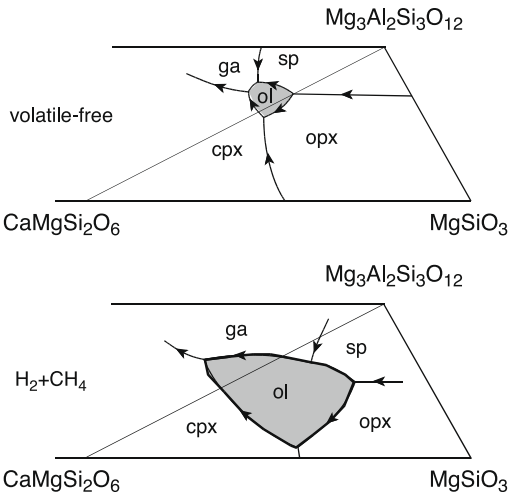

Fig. 11. Simplified liquidus phase relations in portions of the system $CaMgSi_2O6$—$MgSiO_3$—$Mg_3Al_2Si_3O_{12}$ in the presence of $CH_4 + H_2$ gas [$CH_4/(CH_4 + H_2)$~0.8] at 2.8 GPa modified after Eggler and Baker (1982).

5.2. Carbon isotope fractionation between silicate melt and (CH_4 + H_2) fluid

The $\delta^{13}C$ in melts coexisting with ($CH_2 + H_2$) fluid is a function of melt composition and, therefore, melt polymerization (Fig. 2). These polymerization changes are also associated with changes in proportion of CH_4 molecules relative to (C≡C—H)-containing complexes (Fig. 10). Those relationships (Figs. 2 and 10) lead to a simple correlation between changes in $\delta^{13}C$ in the melt coexisting with ($CH_4 + H_2$) fluid and the CH_4/C≡C—H abundance ratio of the melt (Fig. 12). These isotopic changes are consistent with results of thermodynamic modeling of isotope exchange between two phases as a function of the energetics of the C-containing bonds in the individual phases (e.g., Urey, 1947; Bottinga, 1969; Deines, 2002). For example, calculated $^{13}C/^{12}C$ fractionation between atomic C and other C-bearing species such as CO_2, CH_4, graphite, diamond etc. yield carbon isotope fraction factors between 10 and 20‰ under upper mantle temperature conditions (see, for example, Deines, 2002, for review). The $\delta^{13}C$ changes in Fig. 12, reflecting isotope fractionation changes between melt and fluid, are also analogous to experimental results for carbon isotope fractionation between C dissolved in tholeiite melt (in the form of CO_3^{2-} bearing complexes) and coexisting CO_2 fluid (Mattey et al., 1990). The quantitative differences between the latter results and those reported here (Fig. 12) are a reflection of the different symmetries and energy of the carbon isotopes (i.e., energetics of C-containing bonds) in CO_3^{2-} bearing melts (CO_2 dissolves in tholeiite melt in the form of CO_3^{2-} complexes, see for example, Holloway and Blank, 1994) and CO_2 fluid compared with melts that contain (C≡C—H)-bearing complexes and coexist with ($CH_4 + H_2$)-fluid.

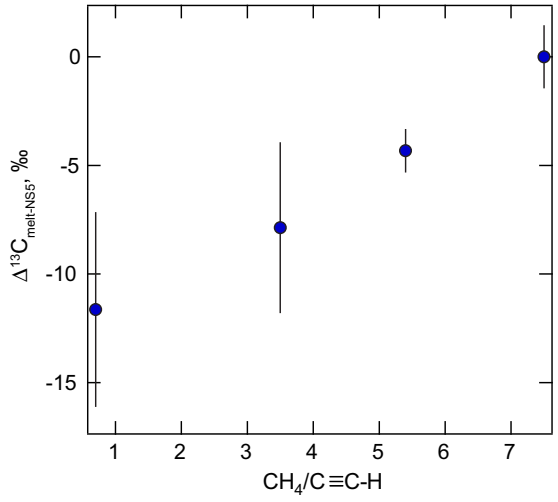

Fig. 12. $\delta^{13}C$ difference and Na_2O—SiO_2 melts as a function of estimated carbon-speciation ratio in the melts (from Figs. 2 and 10). The difference is calculated relative to the value for NS5 composition melts. The individual $\delta^{13}C$ values are given in Table 2. The fluid/melt ratio was constant in all experiments. The error bars are the standard errors (±1σ) of the average of solubility data at 1, 1.5, 2, and 2.5 GPa and replicate analyses for each of the compositions.

ACKNOWLEDGMENTS

We thank reviewers and the AE for their very helpful comments leading to significant improvements of this manuscript. This research was partially supported by the National Science Foundation grants EAR-0405383 and EAR-707861 to B.O.M.

REFERENCES

Alavi S., Ripmeester J. A. and Klug D. D. (2005) NMR shielding constants for hydrogen guest molecules in structure II chlatrates. *J. Chem. Phys.* **123**, 051107.

Behrens H. and Nowak M. (1997) The mechanisms of water diffusion in polymerized silicate melts. *Contrib. Mineral. Petrol.* **126**, 377–385.

Bockris J. O. M., Mackenzie J. D. and Kitchener J. A. (1955) Viscous flow in silica and binary liquid silicates. *Trans. Farad. Soc.* **51**, 1734–1748.

Bohlen S. R. (1984) Equilibria for precise pressure calibration and a frictionless furnace assembly for the piston-cylinder apparatus. *N. Jb. Mineral. Mh.* **84**, 404–412.

Bottinga Y. (1969) Carbon isotope fractionation between graphite, diamond and carbon dioxide. *Earth Planet. Sci. Lett.* **5**, 301–307.

Boyd F. R. and England J. L. (1960) Apparatus for phase equilibrium measurements at pressures up to 50 kilobars and temperatures up to 1750 °C. *J. Geophys. Res.* **65**, 741–748.

Brawer S. A. and White W. B. (1975) Raman spectroscopic investigation of the structure of silicate glasses. I. The binary silicate glasses. *J. Chem. Phys.* **63**, 2421–2432.

Brawer S. A. and White W. B. (1977) Raman spectroscopic investigation of the structure of silicate glasses. II. The soda-alkaline earth-alumina ternary and quaternary glasses. *J. Non-Cryst. Solids* **23**, 261–278.

Brooker R. A., Kohn S. C., Holloway J. R. and McMillan P. F. (2001) Structural controls on the solubility of CO_2 in silicate melts. Part I: bulk solubility data. *Chem. Geol.* **174**, 225–239.

Burton J. C., Sun L., Phphristic M., Lukacs S. J., Log F. H., Feng Z. C. and Ferguson I. T. (1998) Spatial characterization of

doped SiC wafers by Raman spectroscopy. *J. Appl. Phys.* **84**, 6268–6273.

Canil D. (2002) Vanadium in peridotites, mantle and tectonic environments: Archean to present. *Earth Planet. Sci. Lett.* **195**, 75–90.

Carmichael I. S. E., Nicholls J. and Smith A. L. (1970) Silica-activity in igneous rocks. *Am. Mineral.* **55**, 246–263.

Carroll M. R. and Stolper E. M. (1991) Argon solubility and diffusion in silica glass: implication for the solution behavior of molecular gases. *Geochim. Cosmochim. Acta* **55**, 211–226.

Carroll M. R. and Webster J. D. (1994) Solubilities of sulfur, noble gases, nitrogen, chlorine, and fluorine in magmas. In *Volatiles in Magmas* (eds. M. R. Carroll and J. L. Holloway). Mineralogical Society of America, Washington, DC.

Cartigny P. and Ader M. (2003) The nitrogen record of crust-mantle interaction and mantle convection from Archean to present; discussion. *Earth Planet. Sci. Lett.* **216**, 425–432.

Chabot N. L. and Agee C. B. (2003) Core formation in the Earth and the Moon: new experimental constraints from V, Cr, and Mn. *Geochim. Cosmochim. Acta* **67**, 2077–2092.

Chekhmir A. S., Epel'baum M. B. and Simakin A. G. (1988) Water transport in magmas. *Geochem. Int.* **26**, 125–127.

Cody G. D., Mysen B. O. and Lee S. K. (2005) Structure vs. composition: a solid-state 1H and 29Si NMR study of quenched glasses along the Na_2O—SiO_2—H_2O join. *Geochim. Cosmochim. Acta* **69**, 2373–2384.

Cory D. G. and Ritchey W. M. (1988) Suppression of signals from the probe in Bloch decay spectra. *J. Magn. Reson.* **80**, 128–132.

Craig H. (1957) Isotopic standards for carbon and oxygen and correction factors for mass spectrometric analysis of carbon dioxide. *Geochim. Cosmochim. Acta* **12**, 133–149.

Deines P. (2002) The carbon isotope geochemistry of mantle xenoliths. *Earth-Sci. Rev.* **58**, 247–278.

Doremus R. H. (1995) Chemical diffusion in silica glass. *J. Mater. Res.* **10**, 41–69.

Dubessy J., Moissette A., Bakker R. J., Frantz J. D. and Zhang Y. G. (1999) High-temperature Raman spectroscopic study of H_2O—CO_2—CH_4 mixtures in synthetic fluid inclusions; first insights on molecular interactions and analytical implications. *Eur. J. Mineral.* **11**, 23–32.

Dubessy J., Buschaert S., Lamb W., Pironon J. and Thiery R. (2001) Methane-bearing aqueous fluid inclusions; Raman analysis, thermodynamic modeling and application to petroleum basins. *Chem. Geol.* **173**, 193–205.

Eggler D. H. and Baker D. R. (1982) Reduced volatiles in the system C—H—O: implications to mantle melting, fluid formation and diamond genesis. *Adv. Earth Planet. Sci.* **12**, 237–250.

Eugster H. P. and Wones D. R. (1962) Stability relations of the ferruginous biotite, annite. *J. Petrol.* **3**, 82–125.

Fine G. and Stolper E. (1986) Dissolved carbon dioxide in basaltic glasses: concentration and speciation. *Earth Planet. Sci. Lett.* **76**, 263–278.

Florusse L. J., Peters J. C., Schoonman J., Hester K. C., Koh C. A., Dec S. F., Marsh K. N. and Sloan E. D. (2004) Stable low-pressure hydrogen clusters in a binary chlatrate hydrate. *Science* **469–471**.

Furukawa T., Fox K. E. and White W. B. (1981) Raman spectroscopic investigation of the structure of silicate glasses. III. Raman intensities and structural units in sodium silicate glasses. *J. Chem. Phys.* **153**, 3226–3237.

Gessmann C. K. and Rubie D. C. (2000) The origin of the depletions of V, Cr and Mn in the mantles of the Earth and Moon. *Earth Planet. Sci. Lett.* **184**, 95–187.

Getting I. C. and Kennedy G. C. (1970) Effect of pressure on the emf of chromel–alumel and platinum–platinum 90 rhodium 10 thermocouples. *J. Appl. Phys.* **11**, 4552–4562.

Hodges F. N. (1974) The solubility of H_2O in silicate melts. *Carnegie Instn. Wash. Yearbook* **73**, 251–255.

Holloway J. R. (1998) Graphite-melt equilibria during mantle melting; constraints on CO_2 in MORB magmas and the carbon content of the mantle. In *The Degassing of the Earth* (eds. M. R. Carroll, S. C. Kohn and B. J. Wood). Elsevier, Amsterdam, Netherlands.

Holloway J. R. and Jakobsson S. (1986) Volatile solubilities in magmas: transport of volatiles from mantles to planet surfaces. *J. Geophys. Res.* **91**, D505–D508.

Holloway J. R. and Blank J. G. (1994) Application of experimental results to C—O—H species in natural melts. In *Volatiles in Magmas* (eds. M. R. Carroll and J. R. Holloway). Mineralogical Society of America, Washington, DC, USA.

Holloway J. R., Mysen B. O. and Eggler D. H. (1976) The solubility of CO_2 in liquids on the join CaO—MgO—SiO_2—CO_2. *Carnegie Inst. Wash. Yearbook* **75**, 626–631.

Huebner J. S. (1971) Buffering techniques for hydrostatic systems at elevated pressures. In *Research Techniques for High Pressure and High Temperature* (ed. G. C. Ulmer). Springer Verlag, New York.

Jambon A. (1994) Earth degassing and large-scale geochemical cycling of volatile elements. In *Volatiles in Magmas* (eds. M. R. Carroll and J. R. Holloway). Mineralogical Society of America, Washington, DC.

Jambon A., Hartwig W. and Braun O. (1986) Solubility of He, Ne, Ar, Kr and Xe in a basalt melt in the range 1250–1600 °C. Geochemical implications. *Geochim. Cosmochim. Acta* **50**, 401–409.

Kadik A. A., Pineau F., Litvin Y., Jendrzejewski N., Martinez I. and Javoy M. (2004) Formation of carbon and hydrogen species in magmas at low oxygen fugacity. *J. Petrol.* **45**, 1297–1310.

Kasting J. F., Eggler D. H. and Raeburn S. P. (1993) Mantle redox evolution and the oxidation state of the Archean atmosphere. *J. Geol.* **101**, 245–257.

Kohn S. C. (2000) The dissolution mechanisms of water in silicate melts; synthesis of recent data. *Mineral. Mag.* **64**, 389–408.

Kohn S. C., Dupree R. and Smith M. E. (1989) A nuclear magnetic resonance study of the structure of hydrous albite glasses. *Geochim. Cosmochim. Acta* **53**, 2925–2935.

Kohn S. C., Brooker R. A. and Dupree R. (1991) ^{13}C MAS NMR: a method for studying CO_2 speciation in glasses. *Geochim. Cosmochim. Acta* **55**, 3879–3884.

Kubicki J. D., Hemley R. J. and Hofmeister A. M. (1992) Raman and infrared study of pressure-induced structural changes in $MgSiO_3$, $CaMgSi_2O_6$, and $CaSiO_3$ glasses. *Am. Mineral.* **77**, 258–269.

Kushiro I. (1975) On the nature of silicate melt and its significance in magma genesis: regularities in the shift of liquidus boundaries involving olivine pyroxene, and silica materials. *Am. J. Sci.* **275**, 411–431.

Kushiro I. (1976) A new furnace assembly with a small temperature gradient in solid-media, high-pressure apparatus. *Carnegie Instn. Wash. Yearbook* **75**, 832–833.

Lee S. K., Fei Y., Cody G. D. and Mysen B. O. (2003) Structure and disorder of silicate melts at high pressure: ^{17}O 3Q MAS NMR, quantum calculations and thermodynamic modeling. *Geochim. Cosmochim. Acta* **67**, A248.

Libourel G., Marty B. and Humbert F. (2003) Nitrogen solubility in basaltic melt. Part I: effect of oxygen fugacity. *Geochim. Cosmochim. Acta* **67**, 4123–4136.

Luth R. W. and Boettcher A. L. (1986) Hydrogen and the melting of silicates. *Am. Mineral.* **71**, 264–276.

Luth R. W., Mysen B. O. and Virgo D. (1987) Raman spectroscopic study of the behavior of H_2 in the system Na_2O—Al_2O_3—SiO_2—H_2. *Am. Mineral.* **72**, 481–486.

Mao H. K., Bell P. M. and England J. L. (1971) Tensional errors and drift of the thermocouple electromotive force in the single stage, Piston-cylinder apparatus. *Carnegie Instn. Wash. Yearbook* **70**, 281–287.

Matson D. W., Sharma S. and Philpotts J. A. (1986) Raman spectra of some tectosilicates and glasses along the orthoclase-anorthite and nepheline-anorthite joins. *Am. Mineral.* **71**, 694–704.

Mattey D. P., Taylor W. P., Green D. H. and Pillinger C. T. (1990) Carbon isotope fractionation between CO_2 vapour, silicate and carbonate melts: an experimental study to 30 kbar. *Contrib. Mineral. Petrol.* **104**, 492–505.

Mattioli G. S. and Wood B. J. (1986) Upper mantle oxygen fugacity recorded by spinel lherzolites. *Nature* **322**, 626–628.

McCammon C. (2005) Mantle oxidation state and oxygen fugacity: constraints on mantle chemistry, structure and dynamics. In *Earth's Deep Mantle: Structure, Composition, and Evolution* (eds. R. D. van der Hilst, J. D. Bass, J. Matas and J. Trampert). American Geophysical Union, Washington, DC.

McMillan P. (1984) A Raman spectroscopic study of glasses in the system CaO—MgO—SiO_2. *Am. Mineral.* **69**, 645–659.

McMillan P. F. and Remmele R. L. (1986) Hydroxyl sites in SiO_2 glass: a note on infrared and Raman spectra. *Am. Mineral.* **71**, 772–778.

McMillan P. F. and Wolf G. H. (1995) Vibrational spectroscopy of silicate liquids. In *Structure, Dynamics and Properties of Silicate Melts* (eds. J. F. Stebbins, P. F. McMillan and D. B. Dingwell). Mineralogical Society of Washington, Washington, DC.

McMillan P., Piriou B. and Navrotsky A. (1982) A Raman spectroscopic study of glasses along the joins silica-calcium aluminate, silica-sodium aluminate and silica-potassium aluminate. *Geochim. Cosmochim. Acta* **46**, 2021–2037.

McMillan P. F., Poe B. T., Stanton T. R. and Remmele R. L. (1993) A Raman spectroscopic study of H/D isotopically substituted hydrous aluminosilicate glasses. *Phys. Chem. Minerals* **19**, 454–459.

Murphy P. J. and Roberts S. (1995) Laser Raman spectroscopy off differential partitioning in mixed-gas chlatrates in H_2O—CO_2—N_2—CH_4 fluid inclusions. *Geochim. Cosmochim. Acta* **59**, 4809–4824.

Mysen B. O. (1997) Aluminosilicate melts: structure, composition and temperature. *Contrib. Mineral. Petrol.* **127**, 104–118.

Mysen B. O. and Frantz J. D. (1992) Raman spectroscopy of silicate melts at magmatic temperatures: Na_2O—SiO_2, K_2O—SiO_2, and Li_2O—SiO_2 binary compositions in the temperature range 25–1475 °C. *Chem. Geol.* **96**, 321–332.

Mysen B. O. and Cody G. D. (2004) Solubility and solution mechanism of H_2O in alkali silicate melts and glasses at high pressure and temperature. *Geochim. Cosmochim. Acta* **68**, 5113–5126.

Mysen B. O. and Richet P. (2005) *Silicate Glasses and Melts—Properties and Structure*. Elsevier, New York.

Mysen B. O., Yamashita S. and Chertkova N. (2008) Solubility and solution mechanisms of NOH volatiles in silicate melts at high pressure and temperature—amine groups and hydrogen fugacity. *Am. Mineral.* **93**, 1760–1770.

Nakamoto K. (1978) *Infrared and Raman Spectra of Inorganic and Coordination Compounds*. John Wiley & Sons, New York.

Neuville D. R. and Mysen B. O. (1996) Role of aluminum in the silicate network: in-situ, high-temperature study of glasses and melts on the join SiO_2—$NaAlO_2$. *Geochim. Cosmochim. Acta* **60**, 1727–1738.

O'Neill H. S. C. (1991) The origin of the moon and the early history of the earth—a chemical model. Part 2: the earth. *Geochim. Cosmochim. Acta* **55**, 1159–1172.

O'Neill H. S. C., Danil D. and Rubie D. C. (1998) Oxide-metal equilibria to 2500 °C and 25 GPa: implications for core formation and the light component in the Earth's core. *J. Geophys. Res.* **103**, 12260–12339.

Pasteris J. D. (1987) Fluid inclusions in mantle xenoliths. In *Mantle Xenoliths* (ed. P. H. Nixon). John Wiley, New York, pp. 691–707.

Pasteris J. D., Seitz J. C., Wopenka B. and Chou I.-M. (1990) Recent advances in the analysis and interpretation of C—O—H—N fluids by application of laser Raman microspectroscopy. In *Microbeam Analysis* (ed. R. H. Geiss). San Francisco Press Inc., San Francisco.

Pretsch E., Bühlmann P. and Affolter C. (2000) *Structure Determination of Organic Compounds*, third ed. Springer, Berlin.

Righter K. and Drake M. J. (1999) Effect of water on metal-silicate partitioning of siderophile elements: a high pressure and temperature terrestrial magma ocean and core formation. *Earth Planet. Sci. Lett.* **171**, 383–399.

Righter K., Drake M. J. and Yaxley G. (1997) Prediction of siderophile element metal-silicate partition coefficients to 20 GPa and 2800 °C: the effect of pressure, temperature, and oxygen fugacity, and silicate and metallic melt compositions. *Phys. Earth Planet. Int.* **100**, 115–134.

Ryerson F. J. (1985) Oxide solution mechanisms in silicate melts: systematic variations in the activity coefficient of SiO_2. *Geochim. Cosmochim. Acta* **49**, 637–651.

Seifert F. A., Mysen B. O. and Virgo D. (1982) Three-dimensional network structure in the systems SiO_2—$NaAlO_2$, SiO_2—$CaAl_2O_4$ and SiO_2—$MgAl_2O_4$. *Am. Mineral.* **67**, 696–711.

Seitz J. C., Pasteris J. D. and Wopenka B. (1987) Characterization of CO_2—CH_4—H_2O fluid inclusions by microthermometry and laser Raman microprobe spectroscopy: inferences for chlatrate and fluid equilibria. *Geochim. Cosmochim. Acta* **51**, 1651–1664.

Shelby J. E. (1976) Pressure dependence of helium and neon solubility in vitreous silica. *J. Appl. Phys.* **47**, 135–139.

Socrates G. (2001) *Infrared and Raman Characteristic Group Frequencies—Tables and Charts*. John Wiley & Sons, New York.

Stolen R. H. and Walrafen G. E. (1976) Water and its relation to broken bond defects in fused silica. *J. Chem. Phys.* **64**, 2623–2631.

Stolper E. (1982) Water in silicate glasses: an infrared spectroscopic study. *Contr. Mineral. Petrol.* **81**, 1–17.

Strobel T. A., Taylor C. J., Hester K. C., Dec S. F., Koh C. A., Miller K. T. and Sloan E. D. (2006) Molecular hydrogen storage in binary THF-H_2 chlatrate hydrates. *J. Chem. Phys. B* **110**, 17121–17125.

Sykes D. and Kubicki J. D. (1993) A model for H_2O solubility mechanisms in albite melts from infrared spectroscopy and molecular orbital calculations. *Geochim. Cosmochim. Acta* **57**, 1039–1052.

Taylor W. R. and Green D. H. (1987) The petrogenetic role of methane: effect on liquidus phase relations and the solubility mechanisms of reduced C—H volatiles. In *Magmatic Processes: Physicochemical Principles* (ed. B. O. Mysen). Geochemical society, University Park, PA, USA.

Tolstikhin I. N. and Marty B. (1998) The evolution of terrestrial volatiles: a view from helium, argon and nitrogen isotope modeling. *Chem. Geol.* **147**, 27–52.

Urey H. C. (1947) The thermodynamic properties of isotopic substances. *J. Chem. Soc.*, 562–581.

Wright N. and Hunter M. J. (1947) Organosilicon polymers. III. Infrared spectra of the methylpolysiloxanes. *J. Am. Chem. Soc.* **69**, 803–809.

Xue X., Stebbins J. F., Kanzaki M., McMillan P. F. and Poe B. (1991) Pressure-induced silicon coordination and tetrahedral structural changes in alkali oxide-silica melts up to 12 GPa; NMR, Raman, and infrared spectroscopy. *Am. Mineral.* **76**, 8–26.

Yamashita S., Kanzaki M. and Mysen B. O. (2007) In situ observation of silicate speciation in liquids in the system $K_2Si_4O_9$—H_2O at high temperature and high pressure (abstr). In *JPGU Annual Meeting, Chiba City, Japan*.

Zhang Y., Stolper E. M. and Wasserburg G. J. (1991) Diffusion of water in rhyolitic glasses. *Geochim. Cosmochim. Acta* **55**, 441–456.

Associate editor: Peter Ulmer